



Andean headwater and piedmont streams are hot spots of carbon dioxide and methane emissions in the Amazon basin

Gonzalo Chiriboga ^{1,2} & Alberto V. Borges ¹✉

Rivers substantially contribute to global greenhouse gas emissions, yet emissions from headwater streams are poorly constrained. Here, we report dissolved concentrations of carbon dioxide (CO₂), methane (CH₄), and nitrous oxide (N₂O) in Andean headwater and piedmont streams in the Napo River basin in Ecuador, part of the Amazon River catchment. Concentrations increased exponentially with elevation decrease between 3990 and 175 m above sea level. Concentration changes scaled with catchment slope, and were attributed to variations in gas transfer velocity, forest cover, inundation extent, and water temperature. We estimate river emissions across the whole Amazon basin using existing data for the lowland Central Amazon. We find that Andean mountainous headwater and piedmont streams are hotspots of CO₂ and CH₄ emission, with respective areal fluxes being 1.7 and 4.5 higher in headwater streams, and 1.2 and 6.6 higher in piedmont streams than in lowland streams. Together, Andean mountainous headwater and piedmont streams and rivers represented 35% CO₂ and 72% CH₄ of basin scale integrated fluvial diffusive emissions. Conversely, N₂O emissions from headwater and piedmont streams were low compared to lowland streams.

¹Chemical Oceanography Unit, University of Liège, Liège, Belgium. ²Facultad de Ingeniería Química, Universidad Central del Ecuador; Ritter s/n y Bolivia, Quito, Ecuador. ✉email: alberto.borges@uliege.be

Rivers and streams contribute substantially to global natural and anthropogenic emissions of CO₂, CH₄, and N₂O^{1–3}. Estimates of CO₂ emissions from rivers range between 0.7 and 2.9 PgC (10¹⁵ gC) yr⁻¹,^{4–6} and are comparable to the land net CO₂ sink of ~2 PgC yr⁻¹.¹⁷ Estimates of CH₄ emissions from rivers range between 7 and 27 TgCH₄ (10¹² gCH₄) yr⁻¹,⁸ which is lower than the source of CH₄ from freshwater wetlands of ~150 TgCH₄ yr⁻¹.¹⁹ Collectively, aquatic ecosystems (freshwater wetlands, rivers, streams, lakes, ponds, reservoirs, rice paddies, aquaculture ponds, coastal vegetated habitats, estuaries, and ocean) contribute 41% of total global CH₄ emissions from natural and anthropogenic sources⁸. Estimates of N₂O emissions from rivers have been dramatically revised downwards from early estimates of 2,100 GgN₂O-N (10⁹ gN₂O-N) yr⁻¹¹⁰ to 32 GgN₂O-N yr⁻¹.¹¹¹ This large difference is attributable to N₂O riverine emissions being computed from nitrogen (N) deposition and emissions factors that are uncertain¹² and have been revised downwards¹³.

The majority of riverine GHG emissions are from the tropics, ~60–80% for CO₂,^{1,4–6,14,15} ~70% for CH₄,¹⁶ and ~79% for N₂O.¹¹ Yet, the total stream surface area (SSA) in the tropics (24°N–24°S) corresponds to ~44% of the total SSA globally, implying that riverine areal emissions of GHGs (per m²) are higher than in other climatic zones. The higher areal GHG emission rates in the tropics compared to other climate zones is partly related to year-round high temperature that sustains high microbial activity leading to GHG production in soils and in-stream. Additionally, tropical forests with high organic carbon biomass (55% of total¹⁷) and extensive wetlands¹⁸ sustain an important supply of organic carbon to rivers that fuel in-stream microbial production of GHGs.

Yet, the estimates of GHG emissions from tropical rivers and streams remain highly uncertain for several reasons. One being the scarcity of data to characterize the variability within river basins, related for example to differences in river size and land cover on the catchment, but also among river basins, related for example to differences in climatic zones and concomitant differences in land cover. Additionally, emissions of GHGs are disproportionately higher in headwaters and low-order streams¹⁹, including mountainous reaches²⁰. For example, in the Congo River, streams with a Strahler order 1 alone accounted for 62%, 59%, and 45% of basin-wide total CO₂, CH₄, and N₂O emissions, respectively²¹. Streams with Strahler order 1 and 2 accounted, together, for even more, 79%, 77%, and 59% of basin-wide total CO₂, CH₄, and N₂O emissions, respectively²¹. Higher CO₂, CH₄, and N₂O emissions from low-order streams result from a higher input of GHGs from soil-water and ground-water in low-order streams, although highly variable in space and seasonally because soil-water inputs occur during short-lived high-flow events that promote shallow flowpaths²². Additionally, low-order streams,

and in particular mountainous ones are characterized by high values of gas transfer velocity (k)²³. The strong degassing to the atmosphere due to high k values results in concentrations of CO₂ and CH₄ close to equilibrium with the atmosphere in mountainous streams²⁴. Conversely, in lowland river reaches, the presence of wetlands strongly enhances the fluvial riverine CO₂ and CH₄ emissions^{14,15,21,25,26}. There is then a need to describe the spatial variations of GHG fluxes from headwaters to lowlands and understand the underlying drivers. This knowledge should allow choosing the appropriate landscape metrics (catchment slope, land vegetation cover, inundation cover, precipitation, among others) and/or stream attributes (river size, stream gradient, discharge, among others) to statistically model and upscale GHG concentrations and k and compute and integrate riverine GHG fluxes, either at local scale²¹ or globally^{4,5}.

The Amazon is the largest river on the Earth in terms of freshwater discharge and watershed surface area; its basin covers a large portion of the humid Neotropics. The lowland Amazon rivers and streams (channels only at an elevation <500 m) were reported to emit CO₂ at a rate ranging between 0.09⁵ and 0.14²⁷ PgC yr⁻¹. Additionally, headwater Amazonian streams emit CO₂ at a rate ranging between 0.09²⁸ and 0.17⁵ PgC yr⁻¹. The total CO₂ emission from the Amazon running waters (rivers and floodplains) range between 0.5²⁹ and 1.4 PgC yr⁻¹. Rivers and floodplains of the Amazon River entire basin emit CH₄ rate of ~22 TgCH₄ yr⁻¹, but rivers represented about ~0.6% of the total flux, although only integrated for the Solimões–Amazon mainstem³⁰. The CH₄ emissions from large rivers of the Amazon River have been evaluated to 0.5 TgCH₄ yr⁻¹,¹⁶ and CH₄ emissions for the whole lowland Amazon basin (elevation <500 m) to 0.3 TgCH₄ yr⁻¹.³¹ The total emission of CH₄ from Amazonia (including all terrestrial and aquatic compartments) converge to ~40 TgCH₄ yr⁻¹ and have been evaluated with a variety of methods^{32,33}, either based on atmospheric observations (“top down” approach) or upscaling of flux measurements in various relevant components (“bottom up” approach).

Research on GHGs in rivers and streams has mainly focussed on the Central Amazon^{6,15,16,25,28–31,34–39}. Most research has focussed on high-order streams and rivers, and only occasionally in headwater streams^{28,40,41}. Here, we report data of the dissolved CO₂, CH₄, and N₂O concentration in the Andean headwater mountainous and piedmont rivers and streams of the Napo basin in Ecuador (Fig. 1 and Supplementary Fig. 1). We describe gradients of dissolved concentrations of CO₂, CH₄ and N₂O with elevation and their drivers in terms of catchment attributes (slope and land cover), and we model gas emissions at the scale of whole Amazon basin using in addition for lowland rivers a compilation of published data.

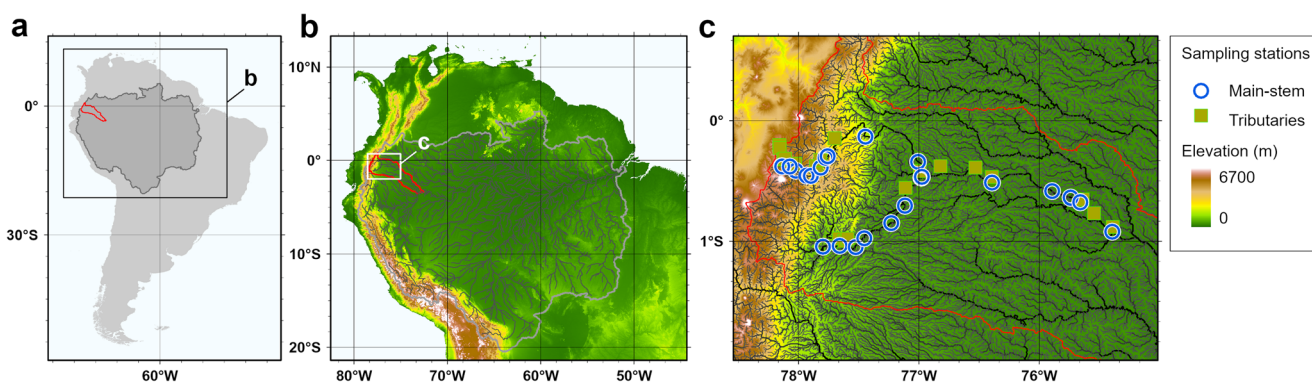


Fig. 1 Location of sampling stations in Andean headwater and piedmont streams of the Amazon basin. **a–c** The outline of the catchment of the Napo River is shown in red, stations in the main-stem are shown by blue circles and in the tributaries by green squares.

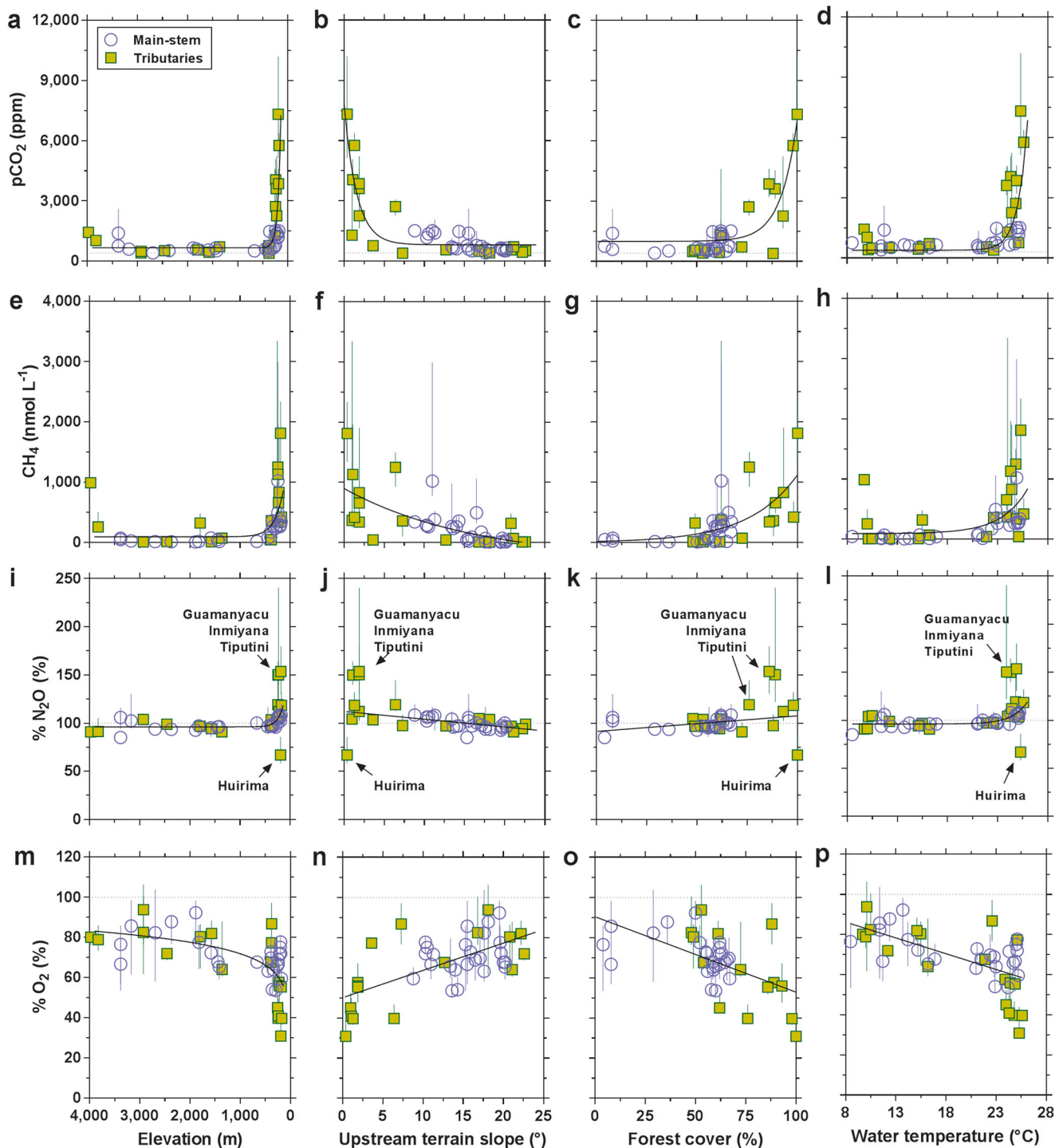


Fig. 2 Strong elevation gradients of $p\text{CO}_2$, CH_4 and $\% \text{N}_2\text{O}$ in the Andean headwater and piedmont streams. Variations of the partial pressure of CO_2 ($p\text{CO}_2$), CH_4 dissolved concentration, N_2O saturation level ($\% \text{N}_2\text{O}$), and oxygen saturation level ($\% \text{O}_2$) in the Napo streams as a function of elevation (**a, e, i, m**), catchment slope (**b, f, j, n**), forest cover (**c, g, k, o**), and water temperature (**d, h, l, p**). Symbols show the median and error bars the interquartile range, stations in the main-stem are shown by blue circles and in the tributaries by green squares, and black lines indicate linear or exponential fits to the data. Solid lines show fits to the data (Supplementary Table 4).

Results and discussion

Altitudinal patterns of stream GHG content. We sampled 25 stations in the mainstem Napo and Coca rivers and 19 stations in the tributaries along an elevation gradient from 3990 m to 175 m above sea level, on 8 occasions from 2018 to 2021 (Fig. 1 and Supplementary Fig. 1). In surface waters of the sampled streams, the values of the partial pressure of CO_2 ($p\text{CO}_2$) ranged

between 152 and 10,873 ppm, and dissolved CH_4 concentrations between 4 and 38,666 nmol L^{-1} (Fig. 2a, e). Values of $p\text{CO}_2$ below atmospheric equilibrium (~ 404 ppm, average of in-situ measurements) were only observed in 22 cases (7% of the total number of observations), while dissolved CH_4 concentration values in surface waters were always above atmospheric equilibrium (~ 2 nmol L^{-1} , based on the global average CH_4 mixing

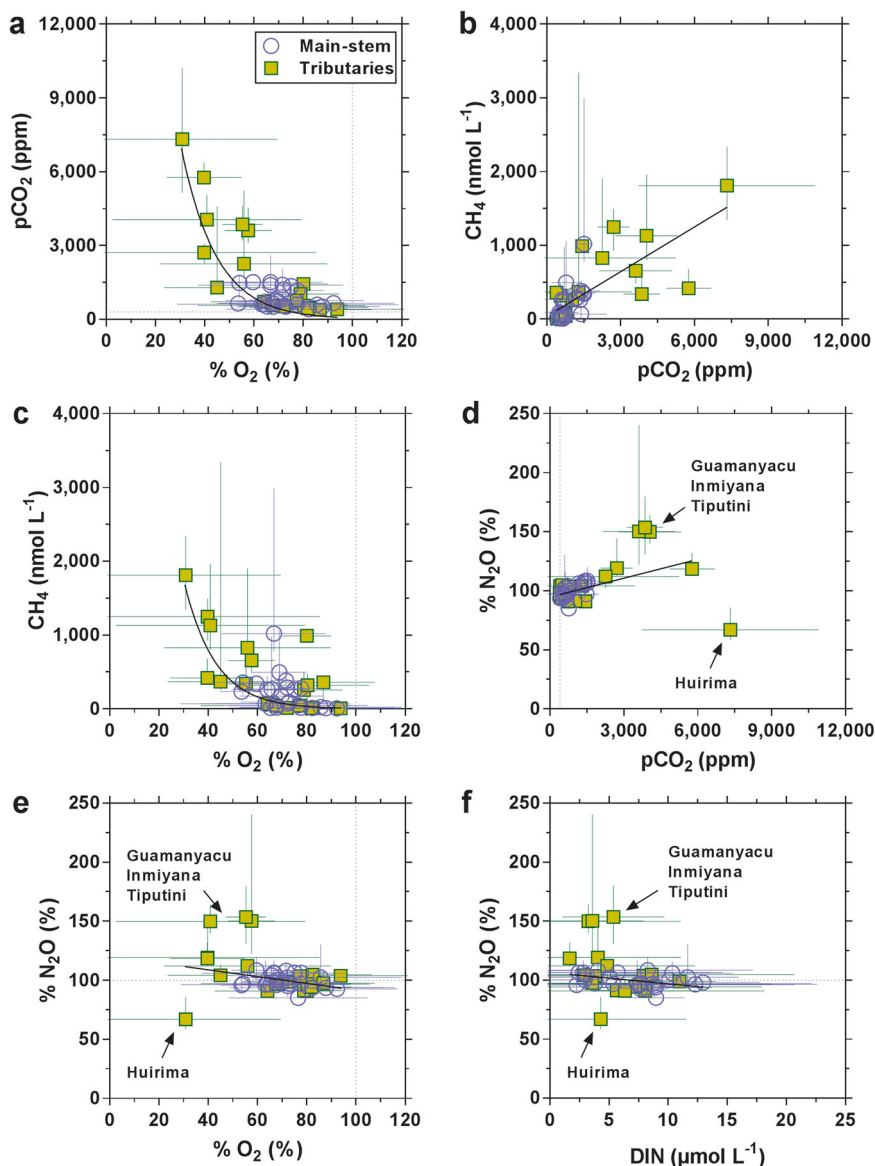


Fig. 3 Strong correlations between $p\text{CO}_2$, CH_4 , $\% \text{N}_2\text{O}$ and $\% \text{O}_2$ in the Andean headwater and piedmont streams. Variations of the partial pressure of CO_2 ($p\text{CO}_2$), CH_4 dissolved concentration, N_2O saturation level ($\% \text{N}_2\text{O}$), as a function of oxygen saturation level ($\% \text{O}_2$) (**a**, **c**, **e**), CH_4 and $\% \text{N}_2\text{O}$ as a function of $p\text{CO}_2$ (**b**, **d**), and $\% \text{N}_2\text{O}$ as a function of dissolved inorganic nitrogen (DIN) (**f**) in the Napo streams. Symbols show the median and error bars the interquartile range, stations in the main-stem are shown by blue circles and in the tributaries by green squares, and black lines indicate linear or exponential fits to the data. Solid lines show fits to the data (Supplementary Table 4).

ratio of 1.9 ppm). The $p\text{CO}_2$ and dissolved CH_4 concentration values in streams at elevations >500 m (median 560 ppm and 17 nmol L^{-1} , respectively) were distinctly lower than at elevations <500 m (median 1280 ppm and 370 nmol L^{-1} , respectively). The $p\text{CO}_2$ and dissolved CH_4 concentration in streams increased exponentially from highlands to lowlands (Fig. 2a, e). The patterns of oxygen saturation level ($\% \text{O}_2$) in streams generally mirrored those of $p\text{CO}_2$ and dissolved CH_4 concentration. The $\% \text{O}_2$ values in streams at elevations >500 m (median 74.4%) were higher than at elevations <500 m (median 63.2%), and $\% \text{O}_2$ decreased exponentially from highlands to lowlands (Fig. 2m).

The $p\text{CO}_2$ and dissolved CH_4 concentration values were positively correlated (Fig. 3b), and they were negatively correlated to $\% \text{O}_2$ (Fig. 3a, c), strongly suggesting that $p\text{CO}_2$ and dissolved CH_4 concentration in streams were controlled by the same combination of input and output processes (that also involved opposite changes of O_2). A likely important output process of CO_2

and CH_4 is the loss to the atmosphere that depends on k . The calculated k values increased with increasing elevation (Supplementary Fig. 2b). Higher k values strongly promoted the emissions of CO_2 and CH_4 to the atmosphere, contributing to drive $p\text{CO}_2$ and dissolved CH_4 concentrations to values close to saturation in the highland streams compared to lowland streams, and could explain in part the decreasing pattern of $p\text{CO}_2$ and dissolved CH_4 concentrations with elevation. A likely important input process of CO_2 and CH_4 is organic matter mineralization in-stream, in fringing wetlands, and in *terra firme* soils of the watershed. Altitudinal changes of organic matter mineralization might have resulted from changes in temperature, soil organic carbon content and land cover. Water temperature strongly increased from highlands to lowlands, from $\sim 13.5^\circ\text{C}$ >500 m elevation to $\sim 24.3^\circ\text{C}$ <500 m (Supplementary Fig. 2a). Rates of respiration^{42,43} and methanogenesis⁴⁴ in soils and riverine sediments are positively related to temperature, suggesting the warmer conditions in the

lowland rivers contributed to higher $p\text{CO}_2$ and dissolved CH_4 concentration values. Indeed, $p\text{CO}_2$ and dissolved CH_4 concentration values also increased exponentially with water temperature (Fig. 2d, h). Changes of water temperature could contribute to explain the decreasing pattern of $p\text{CO}_2$ and dissolved CH_4 concentration with elevation.

There were also changes of land cover with elevation with a transition from a dominance of grasslands in uplands (known as páramos) to forests in lowlands (Supplementary Fig. 3a, b)⁴⁵. Additionally, the presence of fringing wetlands (indicated by inundation extent) strongly increased in the piedmont streams (Supplementary Fig. 3c). Stream $p\text{CO}_2$ and dissolved CH_4 concentration values increased exponentially with forest cover (Fig. 2c, g), and were generally higher where grassland cover was low to zero (Supplementary Fig. 4a, c). Fluvial $p\text{CO}_2$ and dissolved CH_4 concentrations values were positively related to inundation extent in the reach with different slopes for tributaries and main-stem (Supplementary Fig. 4b, d). Fringing wetlands might have a local impact on $p\text{CO}_2$ and dissolved CH_4 concentration in smaller streams (tributaries) in the piedmont region and explain in part the increasing pattern of $p\text{CO}_2$ and dissolved CH_4 concentration with decreasing elevation. Lateral inputs from fringing wetlands strongly influence the fluvial content of dissolved organic carbon (DOC)⁴⁶ and CO_2 ²⁵ in the Central Amazon River. Note that inundation extent was locally high in some of the lowland streams at reach level, but for the whole upstream catchment the inundation extent values were much lower ($\leq 2\%$). Wetlands have been shown to strongly influence $p\text{CO}_2$ and dissolved CH_4 concentration values in lowland African rivers where the wetland cover was higher for the whole upstream catchment¹⁴.

The k values strongly depend on stream gradient and water flow⁴⁷ that both scale with catchment slope, that itself varies with elevation. Vegetation cover (forest and riparian wetlands) and temperature also vary as function of elevation, so, also with catchment slope. Consequently catchment slope could be used as an integrative metric for processes that affect GHGs. Indeed, $p\text{CO}_2$ and dissolved CH_4 concentration values in the sampled streams were found to be negatively related to catchment slope, while $\% \text{O}_2$ was positively related to catchment slope (Fig. 2b, f, n).

The N_2O saturation levels ($\% \text{N}_2\text{O}$) in streams at an altitude > 500 m (median 95.4%) were lower than at elevations < 500 m (median 105.0%) (Fig. 2i). The $\% \text{N}_2\text{O}$ increased exponentially with decreasing elevation and increasing water temperature (Fig. 2i, l), although, in both cases, the exponential increase was less steep than for $p\text{CO}_2$ and dissolved CH_4 concentration (Fig. 2). Lower N_2O in high elevation streams was consistent with reported elevation gradients of N_2O soil-air fluxes in the Ecuadorian Andes, with a soil N_2O sink at high elevation (2200–3010 m) and a N_2O source from soils to the atmosphere at lower elevation (400–1100 m)⁴⁸. The low fluvial $\% \text{N}_2\text{O}$ probably resulted from inputs to river reaches of soil water with low N_2O content. The removal of N_2O in soils was due to complete denitrification (reduction of N_2O to N_2) in highlands related to low soil dissolved inorganic N (DIN) content⁴⁸. Conversely, the N_2O emissions from soils to the atmosphere from lowland soils to the atmosphere was related to high DIN content in soils combined to higher temperature and higher soil water content⁴⁸. The DIN in streams (Supplementary Fig. 5c) was higher in highland streams than in lowland streams, so did not seem to follow the pattern of soil DIN that was higher in lowlands than highlands⁴⁸. The same elevation pattern of stream DIN was reported in Andean streams in Venezuela⁴⁹. High DIN levels were reported in 55 streams in montane forests in Central America and the Caribbean^{50,51}. Large loss of inorganic nitrogen by leakage to streams from unpolluted mature tropical forests occurs ubiquitously across a range of soil types^{50,51}. The higher DIN in highland

streams could be related to higher transfer of DIN from soils to streams related to a lower retention due to differences in vegetation types (grassland versus forest⁵²) or higher catchment slopes that promote soil-river transfer of DIN^{53,54}. In addition, there could have been a higher DIN uptake in the water column by primary producers (phytoplankton or macrophytes) related to decrease in flow and an increase in water residence⁵⁵. The combination of higher stream DIN and low $\% \text{N}_2\text{O}$ in highland streams, and the opposite pattern in lowland streams led to a negative relation between $\% \text{N}_2\text{O}$ and DIN (Fig. 3f). Such a negative relation is unique compared to patterns previously reported, as N_2O content in rivers is in general positively related to DIN^{56–58}.

Four streams showed $\% \text{N}_2\text{O}$ values diverging from general patterns, the Huirima and a cluster of three streams (Guamanyacu, Inmiyana, Tiputini). The Huirima showed distinctly lower $\% \text{N}_2\text{O}$ (67%) than the other lowland streams at equivalent elevations (104–119%) but also the lowest $\% \text{O}_2$ (30.9%) and highest $p\text{CO}_2$ (7317 ppm) values (Fig. 3d, e). The Huirima stream was also characterized by much higher DOC concentrations than all the other streams, suggesting a stronger removal of N_2O by denitrification in soils and/or sediments associated to streams with high DOC and low $\% \text{O}_2$, as also shown in black-water rivers and streams of the Congo basin²¹. The Huirima was characterized by the lowest catchment terrain slope (0.4°) among the sampled streams. Aerial view (Supplementary Fig. 6) showed a dense forest cover and suggested extensive inundation of the Huirima river that probably promoted conditions favorable for complete denitrification and N_2O removal (reducing conditions associated to high DOC and low $\% \text{O}_2$).

The Guamanyacu, Inmiyana, and Tiputini streams drain (in part) oil palm plantations (Supplementary Fig. 7a–c) that could explain the higher stream $\% \text{N}_2\text{O}$ levels (150–153%) compared to surrounding streams (104–119%). In the area, artificial fertilizers are not used in the oil palm plantations, and accordingly, the DIN levels in these streams were comparable to the others at same elevation (Fig. 3f). However, the conversion of natural forest to oil palm plantations itself leads to an increase of N_2O production in soils due to changes in N microbial cycling due to disturbance of the soils⁵⁹. Overall, oil palm plantations did not seem to lose markedly DIN to rivers but there seemed to be intense N_2O production in soils that was transported to streams.

Stream size has been shown to be an important predictor of CO_2 and CH_4 emissions that scale with stream Strahler order in boreal⁶⁰, temperate^{61,62} and tropical²¹ river basins. In highland streams (elevation > 500 m), there were no clear patterns with stream size for $p\text{CO}_2$, dissolved CH_4 concentration, $\% \text{N}_2\text{O}$ and $\% \text{O}_2$ (Supplementary Fig. 8e–h). In the lowland streams, there was an increasing pattern with stream size of $p\text{CO}_2$ and dissolved CH_4 concentration (mirrored by a decreasing pattern of $\% \text{O}_2$) (Supplementary Fig. 8i–l) as frequently observed in other river networks^{21,60–62}. However, when streams were taken together irrespective of altitude, there was no clear relation with stream size for $p\text{CO}_2$, dissolved CH_4 concentrations, $\% \text{N}_2\text{O}$ and $\% \text{O}_2$ (Supplementary Fig. 8a–d), suggesting that the effect of altitudinal gradient overwhelmed the effect of stream size on the variability of these quantities.

Exchange of CO_2 , CH_4 and N_2O with the atmosphere from the Napo river network. The air-water diffusive flux of CO_2 (F_{CO_2}) ranged between -1 and $1074 \text{ mol m}^{-2} \text{ yr}^{-1}$, and was higher in tributaries (median $128 \text{ mol m}^{-2} \text{ yr}^{-1}$) than in the main-stem (median $34 \text{ mol m}^{-2} \text{ yr}^{-1}$). The air-water diffusive flux of CH_4 (F_{CH_4}) ranged between 45 and $8985 \text{ mmol m}^{-2} \text{ yr}^{-1}$, and was generally higher in tributaries (median $999 \text{ mmol m}^{-2} \text{ yr}^{-1}$) than in the main-stem ($332 \text{ mmol m}^{-2} \text{ yr}^{-1}$). Both F_{CO_2} and F_{CH_4}

were inversely correlated to elevation and upstream terrain slope (Supplementary Fig. 9a, b, e, f). The air-water diffusive flux of N_2O (FN_2O) ranged between -23 and 27 $mmol\ m^{-2}\ yr^{-1}$ and did not show marked difference between tributaries and mainstem. There was a general tendency towards a sink of N_2O at an elevation >1000 m with 12 sites showing negative FN_2O values and only 4 showing positive FN_2O values (Supplementary Fig. 9i, j). At an elevation $<1,000$ m the FN_2O values were close to zero (-1.3 to 3 $mmol\ m^{-2}\ yr^{-1}$), except for the Guamanyacu, Inmiyana, and Tiputini streams that showed distinctly positive FN_2O values (9.7 to 21.6 $mmol\ m^{-2}\ yr^{-1}$) and the Huirima that showed a distinctly negative FN_2O value (-7.6 $mmol\ m^{-2}\ yr^{-1}$).

In river geomorphology, the concept of sediment transport capacity has been used to determine if bedload transport is primarily constrained by sediment supply (supply-limited rivers) or river flow hydraulics (transport-limited rivers)⁶³. This concept has been extended by some authors to fluvial CO_2 and CH_4 fluxes^{24,40,64}. The underlying idea being that in highly turbulent systems (high k values) degassing brings gases close to equilibrium with the atmosphere and emissions are close to zero, consequently the gaseous emission is assumed limited by gas availability. Transport- or supply-limitation of the gaseous exchange with the atmosphere can be visualized by plots of gas concentration versus k_{600} ⁶⁴ (Supplementary Fig. 10). At an elevation above 1500 m, computed k_{600} values were higher than $25\ m\ d^{-1}$ while pCO_2 (<746 ppm) and CH_4 (<72 $nmol\ L^{-1}$) values were low indicating supply-limitation of CO_2 and CH_4 emissions (Supplementary Fig. 10a, b). Conversely, in some of the lowland tributaries, particularly high pCO_2 (>1500 ppm) and CH_4 (>500 $nmol\ L^{-1}$) values indicate transport-limitation of CO_2 and CH_4 emissions. There was an exception for both CO_2 and CH_4 , corresponding to high concentrations values ($pCO_2 = 1,395$ ppm and $CH_4 = 320$ $nmol\ L^{-1}$) in highland streams with high k_{600} values (74 and $88\ m\ d^{-1}$, respectively) (indicated by asterisks in Supplementary Figs. 9 and 10). For N_2O , the interpretation of concentration- k_{600} plot in terms of transport- or supply-limitation was not as clear as for CO_2 and CH_4 (Supplementary Fig. 10c). The sampled streams were more or less strongly over-saturated in both CO_2 and CH_4 , consequently the flux was unidirectional from the water to the atmosphere (emission). In contrast, N_2O oscillated between under- and over-saturation, corresponding to a sink or a source of N_2O to the atmosphere, respectively. In the case of a stream acting as a sink of a gas, the supply-limitation is from the atmosphere and not within the stream itself. In this situation, the use of concept of transport capacity as used for sediments⁶³ becomes awkward. At an elevation >1500 m, N_2O concentrations were close to saturation in conjunction with high k_{600} values (Supplementary Fig. 10c). At an elevation below 1500 m, N_2O concentrations markedly above or below saturation were observed in some streams. In this case, the direction and intensity of the N_2O exchange should be more strongly driven by variations of concentrations rather than by those of k_{600} . FCO_2 , FCH_4 and FN_2O strongly correlated with pCO_2 , CH_4 , and $\%N_2O$, respectively, and did not correlate to k_{600} (Supplementary Fig. 9c, g, k, d, h, l), showing that for the whole data-set the variations of gaseous exchanges with the atmosphere were strongly driven by the variations of the concentrations (supply-limitation) rather than by k_{600} (transport-limitation). In highly turbulent systems with high k_{600} values, the gaseous exchanges with the atmosphere bring the concentrations close to equilibrium with the atmosphere, strongly decreasing the flux values that converge to zero.

Comparison of stream GHG content with Central Amazon basin. The pCO_2 values in the rivers and streams of the Central Amazon (median 2950 ppm) were higher than piedmont (median 1280 ppm) and highland (median 555 ppm) streams of the Napo

and there was a general decreasing pattern with elevation and slope (Fig. 4a). In contrast, the CH_4 concentrations in the piedmont streams (median 341 $nmol\ L^{-1}$) were higher than in the rivers and streams of the Central Amazon (median 120 $nmol\ L^{-1}$), that in turn were higher than in the highland streams (median 16 $nmol\ L^{-1}$) (Fig. 4b). There was a general decreasing tendency of CH_4 as function of catchment slope, but at equivalent slope values (at the low end of the range of values), CH_4 concentrations were higher in piedmont streams than lowland stream and rivers. The ratio of CH_4 to CO_2 dissolved concentrations ($CH_4:CO_2$ in $\mu mol:\mu mol$) followed the same patterns as dissolved CH_4 concentration as a function of elevation (Fig. 4e) and catchment slope (Fig. 4f), indicating that for a similar input of CO_2 (lateral input from soils or in-stream mineralization) there was a larger input of CH_4 in piedmont streams than in lowland rivers and streams. The forest cover and water temperatures in piedmont streams are equivalent to those in lowland rivers and streams. The higher dissolved CH_4 concentration in piedmont rivers might result from the combination of relatively higher CH_4 production in the piedmont streams and relatively higher losses of dissolved CH_4 in the lowland rivers. The piedmont region is an area of deposition of suspended particles delivered from the highland streams originating from erosion, up to 30% of the total annual load in the Mamoré river⁶⁵, with an annual freshwater discharge equivalent to the one of the Napo. The deposition of sediments combined by presence of forests in the piedmont region are most probably favorable to high in-stream CH_4 production. In larger lowland river channels that are relatively disconnected from floodplains, the deep water column and strong currents do not promote the accumulation of dissolved CH_4 in the water column, but promote the removal of dissolved CH_4 either by emission of CH_4 to the atmosphere or by microbial oxidation¹⁵.

The only N_2O data in streams and rivers of the Amazon River network were reported by Richey et al.³⁴. When plotted against pCO_2 , the $\%N_2O$ values were higher in the Central Amazon streams and rivers (median 205.6%) compared to piedmont (median 105.0%) and highland (median 95.7%) streams (Supplementary Fig. 11a). We do not have a conclusive hypothesis for the higher $\%N_2O$ in lowland streams and rivers, but the general tendency of higher pCO_2 and N_2O in lowland streams and rivers than in piedmont and highland streams (Supplementary Fig. 11b) suggests more intense mineralization in soils or in-stream leading to higher CO_2 and presumably N_2O levels in rivers in the former systems. The pattern of higher $\%N_2O$ in Central Amazon streams compared to headwater and piedmont streams was also consistent with higher N_2O soil-air fluxes (79 ± 7 $\mu gN\ m^{-2}\ h^{-1}$) in the central part of the basin from oxisols⁶⁶ that are dominant in the Amazon forests⁶⁷ than in piedmont forests (8 ± 12 $\mu gN\ m^{-2}\ h^{-1}$ at 400 m elevation)⁴⁸. Comparatively higher dissolved CH_4 concentrations in piedmont streams than in lowland streams was also evident relative to pCO_2 when compared with the data-set of Richey et al.³⁴ (Supplementary Fig. 11a).

Exchange of CO_2 , CH_4 , and N_2O with the atmosphere from the whole Amazon basin including Andean mountainous and piedmont streams. We used catchment slope as an integrative metric to scale pCO_2 , CH_4 and $\%N_2O$ available in the Amazon River network, as detailed in the Methods section. The k values were derived from stream gradient (slope) and flow velocity⁴⁷, itself computed from discharge⁵, for all the river segments given by RiverATLAS⁶⁸. The areal FCO_2 , FCH_4 , and FN_2O (per m^2) were computed from k and concentrations of CO_2 , CH_4 , N_2O for each river segment of the Amazon catchment given by RiverATLAS ($n = 744,786$) and then integrated with the corresponding SSA.

The piedmont streams accounted for 62% of the total integrated diffusive FCH_4 (0.4 ± 0.1 $TgCH_4\ yr^{-1}$), higher than the

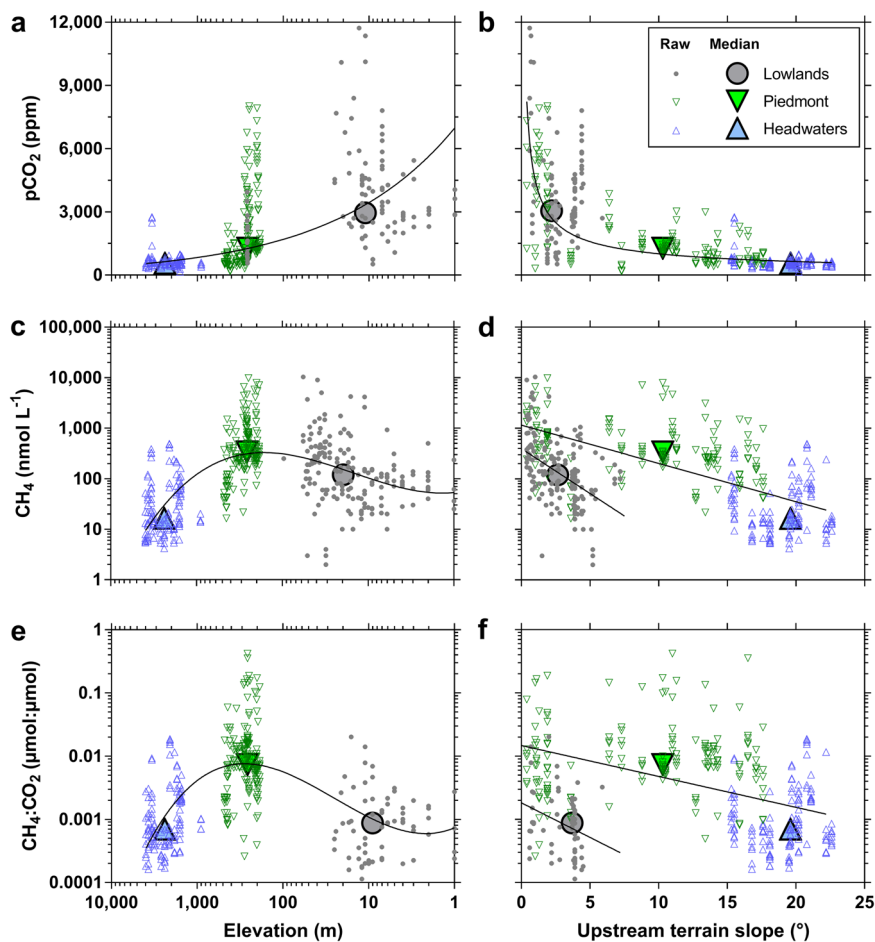


Fig. 4 Strong elevation gradients of $p\text{CO}_2$ and CH_4 in streams and rivers across the whole Amazon basin. Variations of the partial pressure of CO_2 ($p\text{CO}_2$), CH_4 dissolved concentration, and the ratio of CH_4 and CO_2 ($\text{CH}_4:\text{CO}_2$) concentration as function of elevation (**a**, **c**, **e**) and catchment slope (**b**, **d**, **f**). Data in the lowland rivers and streams was compiled from literature for $p\text{CO}_2$ ^{25,35–37,39} and CH_4 ^{15,16,31,39}. For consistency, only studies based on direct measurements of $p\text{CO}_2$ were selected, excluding data derived from the computation of $p\text{CO}_2$ from pH and total alkalinity, as this computation can provide erroneous and unrealistically high $p\text{CO}_2$ values⁷¹³. Data from Scofield et al.³⁸ was excluded because the $p\text{CO}_2$ values reported by these authors in the Negro River (upstream of Manaus) were distinctly lower (710 ppm during low water period and 2608 ppm during higher water period) than other studies in the same system^{25,27,29,36} (~2000–3000 ppm during low water period and ~5000–8000 ppm during higher water period). Small symbols show individual measurements, large symbols indicate the median; the blue triangles show the data in the mountainous headwater streams, green triangles show the data in the piedmont streams, and the grey circles show the data in the lowland streams and rivers, and black lines indicate linear or polynomial fits to the data. Solid lines show fits to the data (Supplementary Table 4).

contribution from lowland rivers (28%), while highland streams accounted for only 10% (Fig. 5b). The diffusive F_{CH_4} per m^2 in highland streams ($1,077 \pm 240 \text{ mmol m}^{-2} \text{ yr}^{-1}$) was 4.5 times higher than in lowland rivers ($237 \pm 79 \text{ mmol m}^{-2} \text{ yr}^{-1}$) despite the fact that dissolved CH_4 concentrations were ~2 times lower (157 ± 35 versus $307 \pm 100 \text{ nmol L}^{-1}$), due to much higher k values (148.8 ± 3.2 versus $14.5 \pm 0.4 \text{ cm h}^{-1}$, Fig. 5e). The diffusive F_{CH_4} per m^2 in piedmont streams ($1,573 \pm 350 \text{ mmol m}^{-2} \text{ yr}^{-1}$) was 6.6 times higher than in lowland rivers ($137 \pm 79 \text{ mmol m}^{-2} \text{ yr}^{-1}$) because of much higher dissolved CH_4 concentrations (797 ± 174 vs. $307 \pm 100 \text{ nmol L}^{-1}$), while k was relatively closer (20.0 ± 0.5 versus $14.5 \pm 0.4 \text{ cm h}^{-1}$).

The integrated F_{CO_2} ($64 \pm 5 \text{ TgC yr}^{-1}$) was dominated by lowland rivers (65%) (Fig. 5a). However, F_{CO_2} per m^2 in highland and piedmont rivers (197 ± 35 and $143 \pm 3 \text{ mol m}^{-2} \text{ yr}^{-1}$) were 1.7 and 1.2 times higher than lowland rivers ($115 \pm 8 \text{ mol m}^{-2} \text{ yr}^{-1}$), respectively (Fig. 5d), due to higher k values, since $p\text{CO}_2$ values were lower in highland streams ($1033 \pm 88 \text{ ppm}$), although comparatively similar in piedmont streams ($2599 \pm 146 \text{ ppm}$) and lowland rivers and streams ($2735 \pm 148 \text{ ppm}$) (Fig. 5g).

The integrated FN_2O ($25 \pm 4 \text{ GgN}_2\text{O-N yr}^{-1}$) was overwhelmingly dominated by lowland rivers and streams (99% of total), while piedmont streams were an extremely small source of N_2O , and highland streams were a very small sink of N_2O (Fig. 5c). The computation of FN_2O is comparatively more uncertain than F_{CH_4} and F_{CO_2} since we extrapolated to all lowland river segments the median % N_2O value given by Richey et al.³⁴, unlike for the other two GHGs for which relations with slope were used to compute concentration values for individual river segments. The median % N_2O value (206%) reported by Richey et al.³⁴ for the Central Amazon rivers and streams was higher than the median value of % N_2O reported in two large African rivers, the Zambezi⁶⁹ and the Congo²¹ rivers of 116% and 131%, respectively. Another study provided a lower % N_2O average value ($134 \pm 25\%$, $n = 131$) in the Solimões and Negro Rivers⁷⁰ than the median % N_2O value (206%) reported by Richey et al.³⁴. Using the lower % N_2O value of 134% for all the lowland rivers provided an integrated FN_2O value for the Amazon River basin of $9 \pm 4 \text{ GgN}_2\text{O-N yr}^{-1}$, which was close to the range of N_2O emissions for the Amazon River basin of 11 to 16 $\text{GgN}_2\text{O-N}$

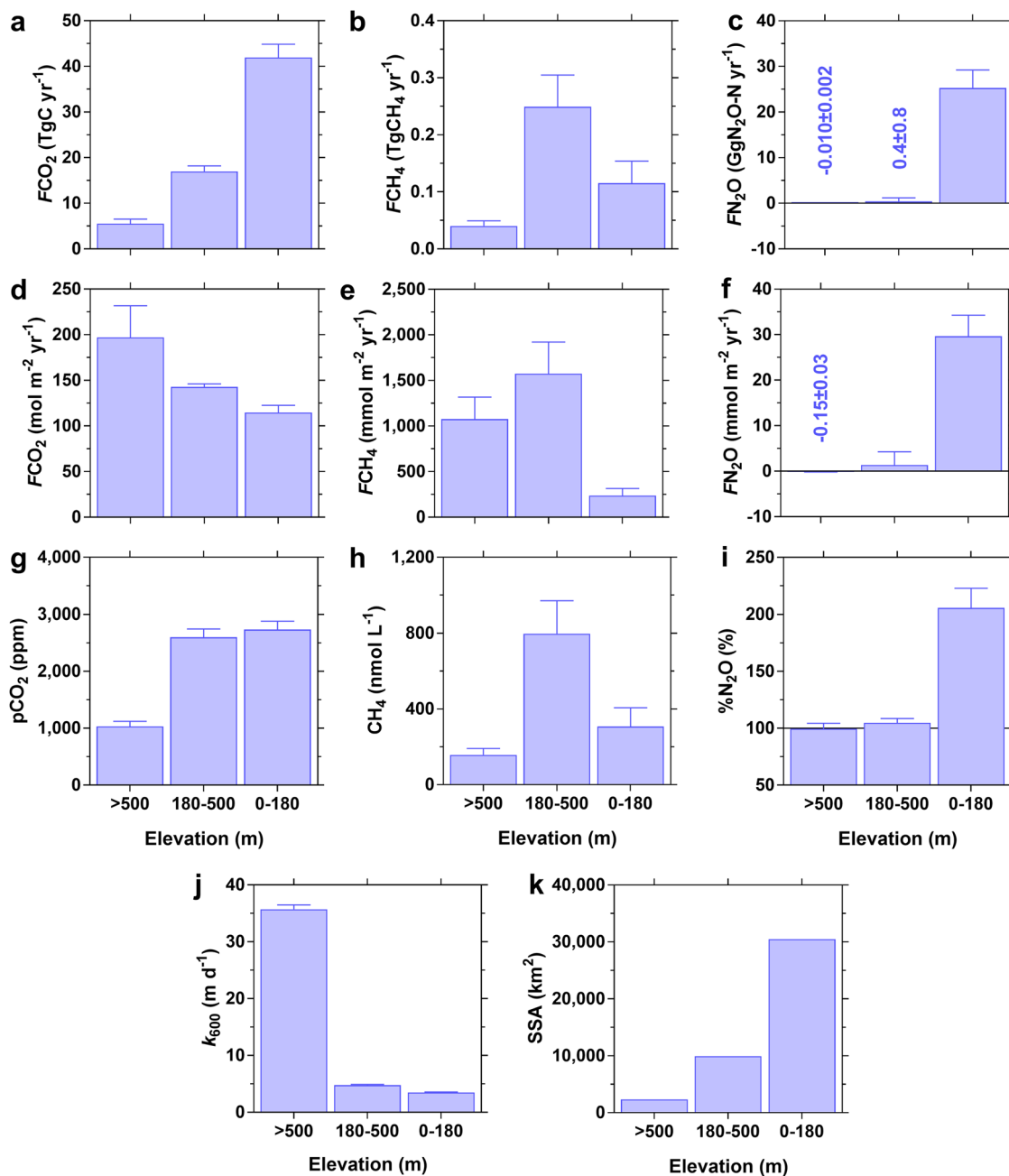


Fig. 5 Andean headwater and piedmont streams are hot spots of CO₂ and CH₄ emissions within the Amazon basin. Air-water fluxes of CO₂ (FCO_2), CH₄ (FCH_4) and N₂O (FN_2O) integrated by area (a–c) and per surface area (m²) (d–f), partial pressure of CO₂ (pCO_2) (g), dissolved CH₄ concentration (h), and N₂O saturation level (%N₂O) (i), gas transfer velocity (k_{600}) (j) and stream surface area (SSA) (k) in the Andean headwater (elevation >500 m), piedmont (elevation 180–500 m) and lowland (elevation <180 m) streams and rivers of the whole Amazon basin. Fluxes were computed from concentrations and k_{600} modelled from attributes of RiverATLAS⁵⁸ for 744,786 river segments. Error bars indicate uncertainties derived from error propagation.

yr⁻¹ modelled from N deposition and emission factors³. The wide range of %N₂O values reported in literature calls for additional data of N₂O in lowland rivers of the Amazon basin for a more accurate evaluation of FN_2O .

The FCO_2 and FCH_4 estimates per m² were consistent (within uncertainties) with those previously reported in the Amazon basin, for lowland basin-wide FCO_2 ^{5,27} and FCH_4 ³¹, FCH_4 for large lowland rivers¹⁶, and the Amazon/Solimões mainstem FCH_4 ³⁰ (Supplementary Table 1). Our lowland basin-wide diffusive FCH_4 per m² is higher than the one reported by Barbosa et al.³¹ because our estimate includes the piedmont rivers with high diffusive FCH_4 values (Fig. 5e) while the estimate of Barbosa et al.³¹ is based on

data from large lowland rivers (Xingu, Tapajós, Madeira, Purus, Juruá, Japurá, Solimões, Negro).

Uncertainties in scaling the exchange of greenhouse gases with the atmosphere. The integrated FCO_2 , FCH_4 , and FN_2O estimates have three sources of uncertainty from each of the terms of the flux computation: the respective modelled dissolved gas concentrations, the k values, and the SSA.

Previous studies that modelled fluvial pCO_2 at continental or global scales either used averaged values per stream order⁶¹ or multi-parametric approaches^{4,5,71} using several catchment properties and climate data as predictors. At the continental scale of

the USA, Lauerwald et al.⁷¹ modelled pCO₂ in streams and rivers with multiple linear regressions (MLR) using catchment slope, mean air temperature, and mean precipitation as predictors. At global scale, Lauerwald et al.⁴ modelled pCO₂ in streams and rivers with MLR using catchment slope, mean air-temperature, land net primary production, and population density as predictors. Also at global scale, Liu et al.⁵ modelled pCO₂ in streams and rivers with a random forest model that used as primary inputs 15 watershed properties including catchment slope, elevation, soil pH, temperature, soil respiration, watershed area, land gross primary production, base saturation, population density, gravel, soil organic carbon, sand, precipitation, land net primary production, and wetland cover (ranked in order of decreasing importance). Note that some of these 15 watershed properties are intimately linked such as land net primary production, gross primary production and soil respiration⁷², or geomorphological variables such as slope and catchment area⁷³, so there could be redundancy in part of the variables used in this random forest model.

There is no standardized procedure to upscale GHG emissions from inland waters which is challenging given the large inherent variability and the comparatively low data coverage. Some studies have used multi-parametric approaches, while we use a simple relation to a single predictor. Complex mathematical approaches do not necessarily provide more reliable results, and, in fact, potentially produce more uncertain estimates⁷⁴. Admittedly, it is unrealistic to model fluvial pCO₂ using a single predictor at continental or global scales. Indeed, at very large spatial scales, it is required to account for strong latitudinal variations as in climate (temperature, precipitation, ice cover) and in soil organic carbon⁷⁵ (among others) that are expected to strongly affect fluvial pCO₂, in addition to local topographic effects that might have a more ubiquitous and uniform effect per latitude (such as the effect of stream slope on *k*). Yet at the scale of a single river basin, it should be possible to reduce the number of variables to model fluvial pCO₂. A simpler model has the advantage to reduce unrealistic results computed outside the bounds of determination of available data, especially from strongly non-linear relationships. We did not find a relation between pCO₂ and dissolved CH₄ concentration and stream order (Supplementary Fig. 8), as used to scale FCO₂ or FCH₄ in some studies at basin or continental scales^{21,60,61}, and we modelled fluvial pCO₂ and dissolved CH₄ concentration based on catchment slope. In the above mentioned three models of fluvial pCO₂ at continental or global scales, catchment slope explained the largest fraction of variance in the MRL^{4,71} or random forest model⁵, and as such was the most important predictor. This high predictive power shows that catchment slope strongly controls fluvial CO₂ content directly or indirectly at multiple levels.

It is well established that topography of a catchment strongly influences hydrological, geomorphological, and biological processes active in the landscape⁷⁶. Catchment slope determines to a large extent broad patterns in the variation of soil organic carbon content^{77–79}, groundwater discharge⁸⁰, stream water residence time⁸¹, and wetland abundance^{82,83}, that, combined, have a major impact on fluvial carbon cycling, including CO₂ and CH₄ dynamics. These processes also determine the inputs to streams and the fluvial content of DOC. Highland steep streams with poorly developed soils and substantial exposed bedrock are characterized by lower fluvial DOC than lowland low-relief streams, and fluvial DOC content correlates to catchment slope^{79,84–86}. Since catchment slope strongly determines fluvial DOC^{79,84–86} and wetland coverage^{82,83}, it is also expected to strongly influence fluvial pCO₂ that has been shown to strongly correlate with DOC^{14,69,87,88} and wetland coverage^{14,15,25} at river basin and continental scales. Wetland coverage can also explain in part the spatial variations of fluvial

dissolved CH₄ concentration^{14,21}. Additionally, the *k* values strongly increase with increasing stream slope^{20,47} that scales with catchment slope⁸⁹ and catchment area⁷³. High *k* values in steeper terrains will promote degassing and equilibration with the atmosphere, while lower *k* values will allow an accumulation of gases in the water. An additional reason to use catchment slope as a predictor is that this variable can be determined with very high confidence based on detailed and precise digital elevation models. Other variables such as land vegetation cover^{90,91} or terrestrial productivity^{92,93} have a relatively large uncertainty especially at finer resolution. We tested if the addition to upstream slope of other variables improved the prediction of pCO₂ (Supplementary Table 2). The MRL including elevation or forest cover in addition of upstream slope did not substantially improve the prediction of pCO₂ compared to the linear regression using upstream slope alone (Supplementary Table 2).

The *k* cannot be measured directly but can be calculated from simultaneous measurements of the air-water gradient of gas concentration and the gas flux. The gas flux in streams can be measured with eddy-covariance, mass balance of deliberate tracers, or floating chambers. Eddy-covariance is the most challenging technically, has been very seldom applied in rivers, and only in large systems^{94,95}. Eddy-covariance measurements require long deployments (weeks-months) due to large data rejection, and are not adapted for “grab-sampling” during spatial surveys of short-duration, as in the present study. The mass balance of deliberate tracers such as argon, propane, SF₆, krypton-85 and tritium allow to derive *k* values at short time intervals and small scales in a non-intrusive way^{23,47}. Floating chamber flux measurements are easy to set-up and inexpensive, however, they might not be adapted for fast flowing small streams as those sampled in the present study. In fast flowing streams, it is required to anchor the floating chamber, leading to an overestimation of flux estimates, due to enhanced turbulence under the chamber^{96,97}. Changes in pressure and temperature inside the chamber additionally affect the flux measurements and *k* estimates⁹⁸. Chamber measurements can advantageously be used to measure gas ebullition which is important for CH₄ but not CO₂ and N₂O, in addition to gas diffusive flux. The *k* parametrization of Raymond et al.⁴⁷ we used in the present study is based on 576 measurements of deliberate gas tracer injections, and has been used in global estimates of CO₂ emission from streams and rivers^{1,4,5}. The *k* values computed with this parameterization have been shown to satisfactorily compare to those derived from chamber measurements by several independent studies in contrasted rivers and streams^{40,60,87,88,99,100}.

To scale FCO₂ and FCH₄, we used the spatial data, including SSA, from RiverATLAS⁶⁸ that provides a standardized compilation of descriptive hydro-environmental information for all river basins of the world at high spatial resolution. The total SSA given by RiverATLAS⁶⁸ globally is 363,000 km², which is lower than the value of 624,000 km² given by Raymond et al.¹ and of 773,000 km² given by the Global River Widths from Landsat (GRWL) data-set¹⁰¹. At the scale of the Amazon basin, the SSA given by RiverATLAS⁶⁸ is also lower than other independent estimates, although the wide range of values reflects their uncertainty (Supplementary Table 3). The SSA of the lowland Amazon basin (<500 m altitude) given by RiverATLAS⁶⁸ (37,972 km²) is between 1.6 and 2.2 times lower than the one reported by Melack²⁷ (60,500–83,000 km²), but 1.4 times lower than the one reported by Liu et al.⁵ (52,640 km²) based on the GRWL data-set¹⁰¹ (Supplementary Table 3). We acknowledge that the integrated fluvial emissions of CO₂, CH₄, and N₂O we computed for the Amazon basin should be considered as conservative, given the lower SSA given by RiverATLAS⁶⁸ compared to other estimates (Supplementary Table 3). Yet, the

general spatial patterns should be correct and the under-estimation of SSA given by RiverATLAS⁶⁸ should not invalidate our major finding regarding the relative importance of the contribution of mountainous and piedmont regions to CO₂ and CH₄ emissions from the Amazon River basin (Fig. 5).

Conclusions

We provide to the best of our knowledge the first large-scale survey across and altitudinal gradient of CO₂, CH₄, and N₂O exchange between Andean mountainous streams of the Amazon River basin and the atmosphere. We showed that these mountainous headwater and piedmont streams were hotspots of CO₂ and CH₄ emissions from the whole Amazon River basin, accounting for a very significant fraction of total emissions (35 and 72% for CO₂ and CH₄ respectively). The present study also provides a baseline evaluation of CO₂, CH₄, and N₂O emissions from headwater mountainous and piedmont streams that could change in response to human alterations and activities on the catchments. In these areas, there are high rates of deforestation and conversion to croplands⁴⁵. There have been concerns about the N₂O emissions from soils to the atmosphere related to oil palm plantations⁵⁹, and here we suggest that part of the N₂O emissions related to oil palm plantations indirectly occur through streams. The oil palm plantations seemed to lead to a strong over-saturation of N₂O (~150%) in streams downstream compared to streams are similar elevations that were characterized by N₂O levels closer to saturation (~110%). Additionally, there has been a boom in hydropower development in the headwaters of the Amazon with potential consequences on aquatic biodiversity¹⁰². Hydropower development could also change sediment transport by rivers to and deposition in piedmont rivers, possibly affecting future CH₄ emissions that were shown here to be particularly high.

Methods

Site description. The Napo River catchment ranges from 100 to 6300 m above sea level, and has a total area of 100,500 km², distributed among Ecuador (59%), Peru (40%), and Colombia (1%)¹⁰³. The Ecuadorian part of the Andean Cordillera is the narrowest within the Central Andes and is characterized by an important volcanic and seismic activity. Below an elevation of 500 m is located a fairly flat and homogeneous forest, part of the Amazonian plains, that covers 82% of the total surface of the Napo basin. The rest of the basin (18%) is constituted by the Andean Cordillera with a vegetation cover composed by grasslands (puna and páramo). The drainage basin receives on average 3200 mm of rainfall per year. At high elevations, rainfall is bimodal and is maximal in April and October and minimal in July–August and in January. In the upper basins, two discharge maxima occur during the two rainfall maxima. In the lowlands, seasonal variability of rainfall and discharge is very weak. The annual discharge of the Napo is 6300 m³ s⁻¹ corresponding to 4% of the Amazon River total discharge at Obidos. The Napo is a ‘white water’ river type characterized by high levels of total suspended matter, and the sediment transport of the Napo River corresponds to 6% of the sediment flow of the Amazon River at Obidos¹⁰³.

Sampling and chemical analysis. Sampling was carried out on eight occasions (October 2018 and 2019, January 2019 and 2020, April 2019 and 2021, July 2019 and 2020) (Supplementary Fig. 1). Stations A1 to A21 were sampled travelling by car, and the others travelling by boat. Sampling was carried out during day-time only (early morning to late afternoon). In some streams, during day-time, oxygen concentrations can strongly increase¹⁰⁴, and, conversely, CO₂ concentrations can decrease¹⁰⁵, in response to aquatic photosynthesis. Fluvial CO₂ emissions can, thus, be under-estimated¹⁰⁵ if data are only acquired during day-time, because night-time CO₂ concentrations and fluxes can be higher than during day-time. Note that a day-time decrease of stream CO₂ and increase of O₂ are not necessarily systematic patterns that depend on the level of in-stream productivity. In lowland streams, rich in DOC, such as in the Congo River network, day-night differences of pCO₂ were low²¹ due to low planktonic primary production¹⁰⁶ and much smaller than the differences among streams (spatial gradients).

Water temperature, specific conductivity, pH, and %O₂ were measured in-situ with a YSI multi-parameter probe (ProPlus). Water for CH₄ and N₂O samples was collected with a sampling device consisting of a 2 L polyethylene bottle with the bottom cut and fitted with a silicone tubing at the stopper¹⁰⁷. Two borosilicate

serum bottles (Weathon) with a volume of 40 ml were filled with the silicone tubing, poisoned with 100 µl of a saturated solution of HgCl₂ and sealed with a butyl stopper and crimped with an aluminium cap. Measurements were made, after over-night equilibration, on an headspace¹⁰⁸ (created by injecting 15 ml of high-purity N₂ into the 40 ml sample bottles), with a gas chromatograph (SRI 8610 C) with a flame ionisation detector for CH₄ and electron capture detector for N₂O calibrated with CH₄:N₂O:N₂ gas mixtures (Air Liquide Belgium) with mixing ratios of 1, 10 and 30 ppm for CH₄, and 0.2, 2.0 and 6.0 ppm for N₂O. The precision of measurement based on duplicate samples was ±10.9% for CH₄ and ±5.8% for N₂O based on 309 replicates.

pCO₂ was measured in the field with a Li-Cor Li-820 infra-red gas analyser based on the headspace technique with 4 polypropylene syringes that were filled directly with river water. The pCO₂ in the atmosphere was measured by injecting ambient air sampled with an additional polypropylene syringe. The Li-Cor Li-820 was calibrated with pure N₂ and CO₂:N₂ gas mixtures (Air Liquide Belgium) of 388, 804, 3707, and 8146 ppm. The final pCO₂ value was computed taking into account the partitioning of CO₂ between water and the headspace, as well as equilibrium with HCO₃⁻¹⁰⁹ using water temperature measured in-stream and after equilibration, and total alkalinity (data not shown). Samples for total alkalinity were conditioned, stored, and analysed as reported elsewhere²¹. The precision of pCO₂ measurement was ±5.2%.

The CO₂ concentration is expressed as partial pressure in parts per million (ppm) and as dissolved concentration for CH₄ (nmol L⁻¹), in accordance with convention in existing topical literature. Variations of N₂O were modest and concentrations fluctuated around atmospheric equilibrium, so data are presented as percent of saturation level (%N₂O, where atmospheric equilibrium corresponds to 100%), computed from the global mean N₂O air mixing ratios given by the Global Monitoring Division (GMD) of the Earth System Research Laboratory (ESRL) of the National Oceanic and Atmospheric Administration (NOAA) (<https://www.esrl.noaa.gov/gmd/hats/combined/N2O.html>), using the Henry's constant¹¹⁰.

Water was collected in the stream surface with a 2 L polyethylene bottle. The water filtered through GF/F Whatman glass fiber filters was collected and further filtered through polyethersulfone syringe encapsulated filters (0.2 µm porosity) for nitrate (NO₃⁻), nitrite (NO₂⁻) and ammonium (NH₄⁺). Samples were stored frozen (-20 °C) in 50 ml polypropylene vials. NO₃⁻ and NO₂⁻ were determined with the sulfanilamide colorimetric with the vanadium reduction method¹¹¹, and NH₄⁺ with the dichloroisocyanurate-salicylate-nitroprussiate colorimetric method¹¹². Detection limits were 0.3, 0.01, and 0.15 µmol L⁻¹ for NH₄⁺, NO₂⁻, and NO₃⁻, respectively. Precisions were ±0.02 µmol L⁻¹, ±0.02 µmol L⁻¹, and ±0.1 µmol L⁻¹ for NH₄⁺, NO₂⁻ and NO₃⁻, respectively.

Computation and upscaling of FCO₂, FCH₄, FN₂O. The dissolved concentrations of CO₂, CH₄, and N₂O were derived from statistical relations as function of catchment slope for each of the river segments in RiverATLAS⁶⁸ ($n = 744,786$). The statistical relations we derived from our own data in the Napo and data available from literature in the lowland rivers and streams of the Central Amazon (Fig. 4).

The pCO₂ (in ppm) was computed according to:

$$\log(\text{pCO}_2) = 3.57(\pm 0.02) - 0.0043(\pm 0.0002) \times \text{CS} \quad (1)$$

$$(r^2 = 0.59, p < 0.0001, n = 473)$$

where CS is the catchment slope ($\times 10^3$).

The CH₄ (in nmol L⁻¹) was computed for an elevation > 180 m according to:

$$\log(\text{CH}_4) = 3.18(\pm 0.08) - 0.0081(\pm 0.0005) \times \text{CS} \quad (2)$$

$$(r^2 = 0.42, p < 0.0001, n = 305)$$

and for an elevation < 180 m according to:

$$\log(\text{CH}_4) = 2.60(\pm 0.08) - 0.0178(\pm 0.003) \times \text{CS} \quad (3)$$

$$(r^2 = 0.21, p < 0.0001, n = 174)$$

The %N₂O (in%) was computed for an elevation > 200 m according to:

$$\% \text{N}_2\text{O} = 106.9(\pm 2.3) - 0.048(\pm 0.014) \times \text{CS} \quad (4)$$

$$(r^2 = 0.04, p = 0.0011, n = 277)$$

and for an elevation of < 200 m the median of values reported by Richey et al.²⁷ (205.6%) was applied uniformly.

To avoid the computation of unrealistic values outside the determination bounds of the regressions, for CS > 200 ($\times 10^3$), a constant value (based on the median of observations within that range of slope values) was applied: 542 ppm for pCO₂ and 96.3% for %N₂O. For CH₄, for an elevation > 180 m, a constant value of 18.5 nmol L⁻¹ was applied for a CS > 200 ($\times 10^3$); for an elevation of < 180 m, a constant value of 60.0 nmol L⁻¹ was applied for a CS > 50 ($\times 10^3$).

The water temperature (WT in $^{\circ}\text{C}$) was computed from the air temperature (AT in $\times 10^{\circ}\text{C}$) from RiverATLAS⁶⁸, according to:

$$WT = 0.00054 \times AT^2 - 0.0964 \times AT + 15.2 \quad (5)$$

$(r^2 = 0.93, n = 371)$

FCO_2 , FCH_4 , FN_2O between surface waters and the atmosphere was computed according to:

$$F = k \times \Delta G \quad (6)$$

where k is the gas transfer velocity (m d^{-1}) and ΔG is the air-water gradient of a given gas.

The k normalized to a Schmidt number (Sc) of 600 (k_{600} in m d^{-1}) was derived from the parameterisation as a function slope and stream water velocity⁴⁷:

$$k_{600} = 2.02 (\pm 0.21) + 2841 (\pm 107) \times V \times S \quad (7)$$

where V is stream velocity (m s^{-1}) and S is stream slope (unitless).

k_{600} was converted to k for the Sc at in-situ temperature⁴⁷ according to:

$$k = k_{600} \times (Sc/600)^{-0.5} \quad (8)$$

The values of S are given by RiverATLAS⁶⁸ and V was computed from discharge (Q in $\text{m}^3 \text{s}^{-1}$) also given by RiverATLAS⁶⁸ according to⁵:

$$\ln(V) = 0.12 \times \ln(Q) - 1.06 \quad (9)$$

A Monte-Carlo error analysis was made by propagating errors (10,000 iterations) on the slope and constant of the equations to compute k_{600} and the gas concentrations (refer to above equations), and an error of $\pm 1^{\circ}\text{C}$ for water temperature.

Data availability

The timestamped and georeferenced data set is available at <https://doi.org/10.5281/zenodo.6527837>.

Received: 16 June 2022; Accepted: 6 March 2023;

Published online: 16 March 2023

References

- Raymond, P. A. et al. Global carbon dioxide emissions from inland waters. *Nature* **503**, 355–359 (2013).
- Stanley, E. H. et al. The ecology of methane in streams and rivers: patterns, controls, and global significance. *Ecol. Mon.* **86**, 146–171 (2016).
- Maa vara, T. et al. Nitrous oxide emissions from inland waters: Are IPCC estimates too high? *Glob. Change Biol.* **25**, 473–488 (2018).
- Lauerwald, R. et al. Spatial patterns in CO_2 evasion from the global river network. *Global Biogeochem. Cycles* **29**, 534–554 (2015).
- Liu, S. et al. The importance of hydrology in routing terrestrial carbon to the atmosphere via global streams and rivers. *Proc. Natl. Acad. Sci. USA* **119**, e2106322119 (2022).
- Sawakuchi, H. O. et al. Carbon dioxide emissions along the lower Amazon River. *Front. Mar. Sci.* **4**, 76 (2017).
- Friedlingstein, P. et al. Global Carbon Budget 2020. *Earth Syst. Sci. Data* **12**, 3269–3340 (2020).
- Rosentreter, J. A. et al. Half of global methane emissions come from highly variable aquatic ecosystem sources. *Nature Geosci.* **14**, 225–230 (2021).
- Saunois, M. et al. The Global Methane Budget 2000–2017. *Earth Syst. Sci. Data* **12**, 1561–1623 (2020).
- Kroeze, C., Dumont, E. & Seitzinger, S. P. Future trends in emissions of N_2O from rivers and estuaries. *J. Integr. Environ. Sci.* **7**, 71–78 (2010).
- Hu, M., Chen, D. & Dahlgren, R. A. Modeling nitrous oxide emission from rivers: a global assessment. *Glob. Change Biol.* **22**, 3566–3582 (2016).
- Clough, T. J., Bertram, J. E., Sherlock, R. R., Leonard, R. L. & Nowicki, B. L. Comparison of measured and EF5-r-derived N_2O fluxes from a spring-fed river. *Glob. Change Biol.* **12**, 477–488 (2006).
- Webb, J. R., Clough, T. J. & Quayle, W. C. A review of indirect N_2O emission factors from artificial agricultural waters. *Environ. Res. Lett.* **16**, 043005 (2021).
- Borges, A. V. et al. Globally significant greenhouse gas emissions from African inland waters. *Nat. Geosci.* **8**, 637–642 (2015a).
- Borges, A. V. et al. Divergent biophysical controls of aquatic CO_2 and CH_4 in the World's two largest rivers. *Sci. Rep.* **5**, 15614 (2015).
- Sawakuchi, H. O. et al. Methane emissions from Amazonian Rivers and their contribution to the global methane budget. *Glob. Change Biol.* **20**, 2829–2840 (2014).
- Pan, Y. et al. A Large and persistent carbon sink in the World's forests. *Science* **333**, 988–993 (2011).
- Fluet-Chouinard, E., Lehner, B., Rebelo, L. M., Papa, F., & Hamilton, S. K. Development of a global inundation map at high spatial resolution from topographic downscaling of coarse-scale remote sensing data. *Remote Sens. Environ.* **158**, 348–361 (2015).
- Marx, A. et al. A review of CO_2 and associated carbon dynamics in headwater streams: A global perspective. *Rev. Geophys.* **55**, 560–585 (2017).
- Horgby, Å. et al. Unexpected large evasion fluxes of carbon dioxide from turbulent streams draining the world's mountains. *Nat. Commun.* **10**, 4888 (2019).
- Borges, A. V. et al. Variations in dissolved greenhouse gases (CO_2 , CH_4 , N_2O) in the Congo River network overwhelmingly driven by fluvial-wetland connectivity. *Biogeochemistry* **167**, 3801–3834 (2019).
- Duvert, C., Butman, D. E., Marx, A., Ribolzi, O. & Hutley, L. B. CO_2 evasion along streams driven by groundwater inputs and geomorphic controls. *Nat. Geosci.* **11**, 813–818 (2018).
- Ulseth, A. J. et al. Distinct air-water gas exchange regimes in low- and high-energy streams. *Nat. Geosci.* **12**, 259–263 (2019).
- Crawford, J. T., Dornblaser, M. M., Stanley, E. H., Clow, D. W. & Striegl, R. G. Source limitation of carbon gas emissions in high-elevation mountain streams and lakes. *J. Geophys. Res. Biogeosci.* **120**, 952–964 (2015).
- Abril, G. et al. Amazon River carbon dioxide outgassing fuelled by wetlands. *Nature* **505**, 395–398 (2014).
- Abril, G. & Borges, A. V. Carbon leaks from flooded land: do we need to re-plumb the inland water active pipe? *Biogeochemistry* **16**, 769–784 (2019).
- Melack, J. M. Aquatic ecosystems. In: Nagy, L., Forsberg, B.R., Artaxo, P. (Eds.), Interactions between Biosphere, Atmosphere and Human Land Use in the Amazon Basin. Springer Berlin Heidelberg, Berlin, Heidelberg, pp. 119–148 (2016).
- Johnson, M. S. et al. CO_2 efflux from Amazonian headwater streams represents a significant fate for deep soil respiration. *Geophys. Res. Lett.* **35**, L17401 (2008).
- Richey, J. E., Melack, J. M., Aufdenkampe, A. K., Ballester, V. M. & Hess, L. Outgassing from Amazonian rivers and wetlands as a large tropical source of atmospheric CO_2 . *Nature* **416**, 617–620 (2002).
- Melack, J. M. et al. Regionalization of methane emissions in the Amazon Basin with microwave remote sensing. *Glob. Change Biol.* **10**, 530–544 (2004).
- Barbosa, P. M. et al. Diffusive methane fluxes from Negro, Solimões and Madeira rivers and fringing lakes in the Amazon basin. *Limnol. Oceanogr.* **61**, S221–S237 (2016).
- Basso, L. S. et al. Amazon methane budget derived from multi-year airborne observations highlights regional variations in emissions. *Commun. Earth Environ.* **2**, 246 (2021).
- Pangala, S. R. et al. Large emissions from floodplain trees close the Amazon methane budget. *Nature* **552**, 230–234 (2017).
- Richey, J. E., Devol, A. H., Wofsy, S. C., Victoria, R. & Riberio, M. N. G. Biogenic gases and the oxidation and reduction of carbon in Amazon River and floodplain waters. *Limnol. Oceanogr.* **33**, 551–561 (1988).
- Rasera, M. F. F. L. et al. Estimating the surface area of small rivers in the southwestern Amazon and their role in CO_2 outgassing. *Earth Interact.* **12**, 1–15 (2008).
- Alin, S. R. et al. Physical controls on carbon dioxide transfer velocity and flux in low-gradient river systems and implications for regional carbon budgets. *J. Geophys. Res.* **116**, G01009 (2011).
- Rasera, M. F. F. L., Krusch, A. V., Richey, J. E., Ballester, M. V. R. & Victória, R. L. Spatial and temporal variability of pCO_2 and CO_2 efflux in seven Amazonian Rivers. *Biogeochemistry* **116**, 241–259 (2013).
- Scofield, V. et al. Carbon dioxide outgassing from Amazonian aquatic ecosystems in the Negro River basin. *Biogeochemistry* **129**, 77–91 (2016).
- Mitchell, C. et al. Radon-traced pore-water as a potential source of CO_2 and CH_4 to receding black and clear water environments in the Amazon Basin. *Limnol. Oceanogr. Lett.* **3**, 375–383 (2018).
- Schneider, C. L. et al. Carbon dioxide (CO_2) fluxes from terrestrial and aquatic environments in a high-altitude tropical catchment. *J. Geophys. Res. Biogeosci.* **125**, e2020JG005844 (2020).
- Whitmore, K. M., Stewart, N., Encalada, A. C., Suárez, E. & Riveros-Iregui, D. A. Spatiotemporal variability of gas transfer velocity in a tropical high-elevation stream using two independent methods. *Ecosphere* **12**, e03647 (2021).
- Kirschbaum, M. The temperature dependence of soil organic matter decomposition, and the effect of global warming on soil organic C storage. *Soil Biol. Biochem.* **27**, 753–760 (1995).
- Cardoso, S. J., Enrich-Prast, A., Pace, M. L. & Roland, F. Do models of organic carbon mineralization extrapolate to warmer tropical sediments? *Limnol. Oceanogr.* **59**, 48–54 (2014).
- Yvon-Durocher, G. et al. Methane fluxes show consistent temperature dependence across microbial to ecosystem scales. *Nature* **507**, 488–491 (2014).
- McClain, M. E. & Naiman, R. J. Andean Influences on the Biogeochemistry and ecology of the Amazon River. *BioScience* **58**, 325–338 (2008).
- McClain, M. E., Richey, J. E., Brandes, J. A. & Pimentel, T. P. Dissolved organic matter and terrestrial-lotic linkages in the central Amazon basin of Brazil. *Glob. Biogeochem. Cycles* **11**, 295–311 (1997).

47. Raymond, P. A. et al. Scaling the gas transfer velocity and hydraulic geometry in streams and small rivers. *Limnol. Oceanogr.: Fluids Environm.* **2**, 41–53 (2012).
48. Pineda, P. A. L. et al. Ideas and perspectives: patterns of soil CO₂, CH₄, and N₂O fluxes along an altitudinal gradient—a pilot study from an Ecuadorian neotropical montane forest. *Biogeosciences* **18**, 413–421 (2021).
49. Allan, J. D. et al. Limnology of Andean piedmont rivers of Venezuela. *J. N. Am. Benthol. Soc.* **25**, 66–81 (2006).
50. Brookshire, E. N. J., Hedin, L. O., Newbold, J. D., Sigman, D. M. & Jackson, J. K. Sustained losses of bioavailable nitrogen from montane tropical forests. *Nat. Geosci.* **5**, 123–126 (2012).
51. Brookshire, E. N. J., Gerber, S., Menge, D. N. L. & Hedin, L. O. Large losses of inorganic nitrogen from tropical rainforests suggest a lack of nitrogen limitation. *Ecol. Lett.* **15**, 9–16 (2012).
52. Templer, P. H. et al. Sinks for nitrogen inputs in terrestrial ecosystems: a meta-analysis of ¹⁵N tracer field studies. *Ecology* **93**, 1816–1829 (2012).
53. Fu, B.-J., Liu, S.-L., Chen, L.-D., Lü, Y.-H. & Qiu, J. Soil quality regime in relation to land cover and slope position across a highly modified slope landscape. *Ecol. Res.* **19**, 111–118 (2004).
54. Becker, J. C. et al. Physiographic gradients determine nutrient concentrations more than land use in a Gulf Slope (USA) river system. *Freshw. Sci.* **33**, 731–744 (2014).
55. Reynolds, C. S. The long, the short and the stalled: on the attributes of phytoplankton selected by physical mixing in lakes and rivers. *Hydrobiologia* **289**, 9–21 (1994).
56. Rosamond, M. S., Thuss, S. J. & Schiff, S. L. Dependence of riverine nitrous oxide emissions on dissolved oxygen levels. *Nat. Geosci.* **5**, 715–718 (2012).
57. Herreid, A. M., Wymore, A. S., Varner, R. K., Potter, J. D. & McDowell, W. H. Divergent controls on stream greenhouse gas concentrations across a land-use gradient. *Ecosystems* **24**, 1299–1316 (2021).
58. Zhang, L. et al. Unexpectedly minor nitrous oxide emissions from fluvial networks draining permafrost catchments of the East Qinghai-Tibet Plateau. *Nat. Commun.* **13**, 950 (2022).
59. Skiba, U., Hergoualc'h, K., Drewer, J., Meijide, A. & Knohl, A. Oil palm plantations are large sources of nitrous oxide, but where are the data to quantify the impact on global warming? *Curr. Opin. Environ. Sustain.* **47**, 81–88 (2020).
60. Wallin, M. B. et al. Carbon dioxide and methane emissions of Swedish low-order streams - a national estimate and lessons learnt from more than a decade of observations. *Limnol. Oceanogr. Lett.* **3**, 156–167 (2018).
61. Butman, D. & Raymond, P. A. Significant efflux of carbon dioxide from streams and rivers in the United States. *Nat. Geosci.* **4**, 839–842 (2011).
62. Borges, A. V. et al. Effects of agricultural land use on fluvial carbon dioxide, methane and nitrous oxide concentrations in a large European river, the Meuse (Belgium). *Sci. Total Environ.* **610–611**, 342–355 (2018).
63. Wainwright, J. et al. The concept of transport capacity in geomorphology. *Rev. Geophys.* **53**, 1155–1202 (2015).
64. Rocher-Ros, G., Sponseller, R. A., Lidberg, W., Mörth, C.-M. & Giesler, R. Landscape process domains drive patterns of CO₂ evasion from river networks. *Limnol. Oceanogr. Lett.* **4**, 87–95 (2019).
65. Vauchel, P. et al. (2017) A reassessment of the suspended sediment load in the Madeira River basin from the Andes of Peru and Bolivia to the Amazon River in Brazil, based on 10 years of data from the HYBAM monitoring programme. *J. Hydrol.* **553**, 35–48 (2017).
66. Keller, M. et al. Soil-atmosphere exchange of nitrous oxide, nitric oxide, methane and carbon dioxide in logged and undisturbed forest in Tapajós National Forest, Brazil. *Earth Interact.* **9**, 1–28 (2005).
67. Bernoux, M., Arrouays, D., Cerri, C. C. & Bourennane, H. Modeling vertical distribution of carbon in oxisols of the western Brazilian Amazon (Rondonia). *Soil Sci.* **163**, 941–951 (1998).
68. Linke, S. et al. Global hydro-environmental sub-basin and river reach characteristics at high spatial resolution. *Sci. Data* **6**, 283 (2019).
69. Teodoru, C. et al. Spatial variability and temporal dynamics of greenhouse gas (CO₂, CH₄, N₂O) concentrations and fluxes along the Zambesi River mainstem and major tributaries. *Biogeosciences* **12**, 2431–2453 (2015).
70. Oliveira, C.B. et al. Preliminary measurements of N₂O partial pressures in rivers of Amazon Basin, Brazil, American Geophysical Union, Fall Meeting 2006, abstract id. B31C-B31126 (2006).
71. Lauerwald, R., Hartmann, J., Moosdorf, N., Kempe, S. & Raymond, P. A. What controls the spatial patterns of the riverine carbonate system? - A case study for North America. *Chem. Geol.* **337–338**, 114–127 (2013).
72. Chen, S., Zou, J., Hu, Z., Chen, H. & Lu, Y. Global annual soil respiration in relation to climate, soil properties and vegetation characteristics: Summary of available data. *Agric. For. Meteorol.* **198–199**, 335–346 (2014).
73. Flint, J. J. Stream gradient as a function of order, magnitude, and discharge. *Water Resour. Res.* **10**, 969–973 (1974).
74. Puy, A. et al. Models with higher effective dimensions tend to produce more uncertain estimates. *Sci. Adv.* **8**, <https://doi.org/10.1126/sciadv.abn9450> (2022).
75. Langeveld, J. et al. Estimating dissolved carbon concentrations in global soils: a global database and model. *SN Appl. Sci.* **2**, 1–21 (2020). 1626.
76. Moore, I. D., Grayson, R. B. & Ladson, A. R. Digital terrain modelling: A review of hydrological, geomorphological, and biological applications. *Hydrol. Process.* **5**, 3–30 (1991).
77. Thompson, J. A. & Kolka, R. K. Soil carbon storage estimation in a forested watershed using quantitative soil-landscape modeling. *Soil Sci. Soc. Am. J.* **69**, 1086–1093 (2005).
78. de Brogniez, D. et al. A map of the topsoil organic carbon content of Europe generated by a generalized additive model. *Eur. J. Soil Sci.* **66**, 121–134 (2015).
79. Connolly, C. T. et al. Watershed slope as a predictor of fluvial dissolved organic matter and nitrate concentrations across geographical space and catchment size in the Arctic. *Environ. Res. Lett.* **13**, 1–9 (2018). 104015.
80. Leach, J. A. et al. Evaluating topography-based predictions of shallow lateral groundwater discharge zones for a boreal lake-stream system. *Water Resour. Res.* **53**, 5420–5543 (2017).
81. McGuire, K. J. et al. The role of topography on catchment-scale water residence time. *Water Resour. Res.* **41**, W05002 (2005).
82. Merot, P. et al. Testing a climato-topographic index for predicting wetlands distribution along an European climate gradient. *Ecol. Modell.* **163**, 51–71 (2003).
83. Rodhe, A. & Seibert, J. Wetland occurrence in relation to topography: a test of topographic indices as moisture indicators. *Agric. For. Meteorol.* **98–99**, 325–340 (1999).
84. Mulholland, P. J. Dissolved organic matter concentration and flux in streams. *J. North Am. Benthol. Soc.* **16**, 131–141 (1997).
85. Parry, L. E. et al. The influence of slope and peatland vegetation type on riverine dissolved organic carbon and water colour at different scales. *Sci. Total Environ.* **527–528**, 530–539 (2015).
86. Harms, T. K. et al. Catchment influence on nitrate and dissolved organic matter in Alaskan streams across a latitudinal gradient. *J. Geophys. Res. Biogeosci.* **121**, 350–369 (2016).
87. Ran, L. et al. Riverine CO₂ emissions in the Wuding River catchment on the Loess Plateau: Environmental controls and dam impoundment impact. *J. Geophys. Res. Biogeosci.* **122**, 1439–1455 (2017).
88. Rasilo, T., Hutchins, R. H. S., Ruiz-González, C. & del Giorgio, P. A. Transport and transformation of soil-derived CO₂, CH₄ and DOC sustain CO₂ supersaturation in small boreal streams. *Sci. Total Environ.* **579**, 902–912 (2017).
89. Willgoose, G. A physical explanation for an observed area-slope-elevation relationship for catchments with declining relief. *Water Resour. Res.* **30**, 151–159 (1994).
90. Hua, T. et al. Spatial consistency assessments for global land-cover datasets: A comparison among GLC2000, CCI LC, MCD12, GLOBCOVER and GLCNMO. *Remote Sens.* **10**, 1846 (2018).
91. Gao, H., Jia, G. S. & Fu, Y. Identifying and quantifying pixel-level uncertainty among major satellite derived global land cover products. *J. Meteor. Res.* **34**, 806–821 (2020).
92. Liu, Y. et al. Satellite-derived LAI products exhibit large discrepancies and can lead to substantial uncertainty in simulated carbon and water fluxes. *Remote Sens. Environ.* **206**, 174–188 (2018).
93. Zhang, Y. & Ye, A. Uncertainty analysis of multiple terrestrial gross primary productivity products. *Glob. Ecol. Biogeogr.* **31**, 2204–2218 (2022).
94. Huotari, J., Haapanala, S., Pumpanen, J., Vesala, T. & Ojala, A. Efficient gas exchange between a boreal river and the atmosphere. *Geophys. Res. Lett.* **40**, 5683–5686 (2013).
95. Van Dam, B. R., Edson, J. B. & Tobias, C. Parameterizing air-water gas exchange in the shallow, microtidal New River estuary. *J. Geophys. Res. Biogeosci.* **124**, 2351–2363 (2019).
96. Lorke, A. et al. Technical note: drifting versus anchored flux chambers for measuring greenhouse gas emissions from running waters. *Biogeosciences* **12**, 7013–7024 (2015).
97. Vingiani, F. et al. Evaluating stream CO₂ outgassing via drifting and anchored flux chambers in a controlled flume experiment. *Biogeosciences* **18**, 1223–1240 (2021).
98. Belanger, T. V. & Kozum, E. A. Critique of floating dome technique for estimating reaeration rates. *J. Environ. Eng.* **117**, 144–150 (1991).
99. Campeau, A., Lapierre, J.-F., Vachon, D. & del Giorgio, P.A. Regional contribution of CO₂ and CH₄ fluxes from the fluvial network in a lowland boreal landscape of Québec. *Glob. Biogeochem. Cycles* **28**, <https://doi.org/10.1002/2013GB004685> (2014).
100. Lim, A. G. et al. Carbon emission and export from the Ket River, western Siberia. *Biogeosciences* **19**, 5859–5877 (2022).
101. Allen, G. H. & Pavelsky, T. M. Global extent of rivers and streams. *Science* **361**, 585–588 (2018).
102. Anderson, E. P. et al. Fragmentation of Andes-to-Amazon connectivity by hydropower dams. *Sci. Adv.* **4**, aao1642 (2018).
103. Laraque, A. et al. Sediment budget of the Napo River, Amazon basin, Ecuador and Peru. *Hydrol. Process.* **23**, 3509–3524 (2009).

104. Hall, R. O., Tank, J. L., Baker, M. A., Rosi-Marshall, E. J. & Hotchkiss, E. R. Metabolism, gas exchange, and carbon spiraling in rivers. *Ecosystems* **19**, 73–86 (2016).
105. Gómez-Gener, L. et al. Global carbon dioxide efflux from rivers enhanced by high nocturnal emissions. *Nat. Geosci.* **14**, 289–294 (2021).
106. Descy, J.-P. et al. Phytoplankton dynamics in the Congo River. *Freshw. Biol.* **62**, 87–101 (2017).
107. Abril, G., Commarieu, M.-V. & Guérin, F. Enhanced methane oxidation in an estuarine turbidity maximum. *Limnol. Oceanogr.* **52**, 470–475 (2007).
108. Weiss, R. F. Determinations of carbon dioxide and methane by dual catalyst flame ionization chromatography and nitrous oxide by electron capture chromatography. *J. Chromatogr. Sci.* **19**, 611–616 (1981).
109. Dickson, A.G., Sabine, C.L. & Christian, J.R. (Eds.) Guide to best practices for ocean CO₂ measurements. PICES Special Publication 3, 191 pp. (2007).
110. Weiss, R. F. & Price, B. A. Nitrous oxide solubility in water and seawater. *Mar. Chem.* **8**, 347–359 (1980).
111. American Public Health Association. Standard methods for the examination of water and wastewater, (APHA, 1998).
112. Standing committee of Analysts (1981). Ammonia in waters. Methods for the examination of waters and associated materials. 16 pp (HMSO, 1981).
113. Abril, G. et al. Technical Note: Large overestimation of calculated pCO₂ in acidic, organic-rich freshwaters. *Biogeosciences* **12**, 67–78 (2015).

Acknowledgements

We thank three anonymous reviewers for constructive comments on the initial manuscript. This research was funded by the *Académie de recherche et d'enseignement supérieur* (ARES). A.V.B. is a research director at the *Fonds National de la Recherche Scientifique*.

Author contributions

A.V.B. designed the research and analyzed the data. G.C. collected and analyzed the samples. A.V.B. and G.C. equally contributed to drafting the manuscript.

Competing interests

The authors declare no competing interests.

Additional information

Supplementary information The online version contains supplementary material available at <https://doi.org/10.1038/s43247-023-00745-1>.

Correspondence and requests for materials should be addressed to Alberto V. Borges.

Peer review information *Communications Earth & Environment* thanks Nicholas Marzolf and the other, anonymous, reviewer(s) for their contribution to the peer review of this work. Primary Handling Editor: Clare Davis. Peer reviewer reports are available.

Reprints and permission information is available at <http://www.nature.com/reprints>

Publisher's note Springer Nature remains neutral with regard to jurisdictional claims in published maps and institutional affiliations.



Open Access This article is licensed under a Creative Commons Attribution 4.0 International License, which permits use, sharing, adaptation, distribution and reproduction in any medium or format, as long as you give appropriate credit to the original author(s) and the source, provide a link to the Creative Commons license, and indicate if changes were made. The images or other third party material in this article are included in the article's Creative Commons license, unless indicated otherwise in a credit line to the material. If material is not included in the article's Creative Commons license and your intended use is not permitted by statutory regulation or exceeds the permitted use, you will need to obtain permission directly from the copyright holder. To view a copy of this license, visit <http://creativecommons.org/licenses/by/4.0/>.

© The Author(s) 2023